Journal of Materials Chemistry C

RSC Publishing

PAPER

View Article Online
View Journal | View Issue

Cite this: J. Mater. Chem. C, 2013, 1, 7748

Enhanced crystallinity and film retention of P3HT thin-films for efficient organic solar cells by use of preformed nanofibers in solution†

Nico Seidler,[a] Giovanni Mattia Lazzerini,[a] Giovanni Li Destri,[b] Giovanni Marletta[b] and Franco Cacialli*[a]

We report the preparation of films of poly(3-hexylthiophene) nanofibers suitable for fabrication of efficient multilayer solar cells by successive deposition of donor and acceptor layers from the same solvent. The nanofibers are obtained by addition of di-*tert*-butyl peroxide (DTBP) to a solution of P3HT in chlorobenzene. Interestingly, by varying the concentration of DTBP we are able to control both crystallinity and film retention of the spin-cast films. We also investigate the influence of the DTBP-induced crystallization on charge transport by thin-film transistor measurements, and find a more than five-fold increase in the hole mobility of nanofiber films compared to pure P3HT. We attribute this effect to the synergistic effects of increased crystallinity of the fibers and the formation of micrometer-sized fiber networks. We further demonstrate how it is possible to make use of the high film retention to fabricate photovoltaic devices by subsequent deposition of [6,6]-phenyl-C61-butyric acid methyl ester (PCBM) from a chlorobenzene solution on top of the nanofiber film. The presence of a relatively large crystalline phase strongly affects the diffusion behavior of PCBM into the P3HT film, resulting in a morphology which is different from that of common bulk heterojunction solar cells and resembles a bilayer structure, as can be inferred from comparison of the external quantum efficiency spectra. However, a high power conversion efficiency of 2.3% suggests that there is still a significant intermixing of the two materials taking place.

Received 4th July 2013
Accepted 28th September 2013

DOI: 10.1039/c3tc31284d

www.rsc.org/MaterialsC

1. Introduction

Organic semiconductors have attracted great interest for photovoltaic applications due to their potential to be manufactured at low cost and on a large variety of substrates.[1–4] To achieve large-scale production, it is crucial to develop a highly reproducible fabrication procedure that can be incorporated in a roll-to-roll process, and that avoids high temperature treatments to ensure compatibility with flexible substrates. One of the most extensively investigated systems for this purpose is a heterojunction of poly(3-hexylthiophene) (P3HT) as electron donor and a fullerene complex as electron acceptor, such as [6,6]-phenyl-C61-butyric acid methyl ester (PCBM). Particular attention has been given to the influence of intrinsic photophysical properties and aggregation behavior of P3HT, since it is known that the degree of molecular order of this component of the active layer plays an important role in the resulting performance of the photovoltaic device.[5,6]

It has been found that thin-films of regioregular P3HT deposited from solution consist of a semi-crystalline fraction of highly ordered π–π stacks with a typical stacking distance of 3.8 Å, and a less ordered, amorphous fraction.[7,8] Several factors are known to influence this aggregation behavior, including the choice of solvent and the film preparation method, as well as macromolecular properties of P3HT, such as molecular weight, regioregularity, and polydispersity.[9–14]

Ihn and coworkers first described that poly(3-alkylthiophenes) can form macroscopic structures in the shape of long whiskers of the length of several micrometers.[15] Their method of slowly cooling a solution of P3HT in a poor solvent has been further investigated by other groups,[16,17] and similar methods were developed involving non-solvents as additives,[18–21] and the exposure to ultrasound.[22,23]

One possibility to achieve a controllable fabrication process and to add a degree of freedom in the complexity of device structures is the sequential deposition of multiple layers by insolubilization of the previous layers by cross-linking.[24–28] Just few reports exist so far on the cross-linking of P3HT in order to obtain insoluble layers of P3HT that can be used to gain better

[a]Department of Physics and Astronomy and London Centre for Nanotechnology, University College London, Gower Street, London WC1E 6BT, UK. E-mail: f.cacialli@ucl.ac.uk

[b]Laboratory for Molecular Surfaces and Nanotechnology (LAMSUN), Department of Chemical Sciences, University of Catania, Viale A. Doria 6, 95125 Catania, Italy

† Electronic supplementary information (ESI) available. See DOI: 10.1039/c3tc31284d

control over the morphology in solution processed donor–acceptor solar cells.[29]

Gearba and coworkers reported on thermally cross-linked P3HT by the use of di-*tert*-butyl peroxide (DTBP), in analogy to a process commonly used in rubber industry to cross-link polyethylene.[30–32] By adding DTBP directly to a solution of P3HT in chlorobenzene, and by annealing the films spin-cast from this solution, they observed the films to become insoluble with increasing peroxide concentration. They show a higher crystallinity of the film and a higher conductivity as well as a slight blue-shift of the absorption spectrum, and concluded in favor of a cross-linking process instead of a self-assembly of the P3HT chains, albeit without the support of a surface morphology study.

In this work, we show that it is possible to control the crystallinity and retention of thin-films of P3HT by using DTBP as an additive, even when processing at room temperature. We demonstrate how the nanoscopic and macroscopic morphology is influenced by the amount of peroxide added to the solution and we correlate this to the performance of both thin-film transistors (TFT) and solar cells. Using UV-vis absorption measurements and grazing-incidence X-ray diffraction (GIXD), we prove an increase in crystallinity upon addition of DTBP to a solution of P3HT in chlorobenzene. Interestingly, X-ray photoelectron spectroscopy (XPS) shows that the addition of the peroxide does not result in detectable oxidation of the polymer. Atomic force microscopy (AFM) images reveal the formation of P3HT fibers up to a length of several micrometers. In addition, we investigate the influence of the peroxide addition on the charge transport properties by thin-film transistor measurements, and find a progressive increase in the field-effect mobility with increasing DTBP concentration. We are able to control the retention of the films by adjusting the amount of DTBP added to the solution and make use of this to fabricate efficient solar cells by successively depositing the donor and acceptor layer from the same solvent, using PCBM as an electron acceptor. Such cells feature a power conversion efficiency of 2.3%. Since these cells have not been optimized in terms of layer thickness and other processing parameters, we consider there are good prospects for improvement.

2. Experimental

All materials used, including regioregular P3HT (number average molecular weight of 30 000–60 000), PCBM, DTBP, and all solvents were purchased from Sigma-Aldrich and used as received without further purification. The P3HT solutions were prepared under ambient conditions by solving 10 mg ml^{-1} P3HT in chlorobenzene (corresponding to 0.9% by weight), heating the solution to 75 °C for 1 h, and then leaving it on the stirrer for about 12 h at room temperature (~21 °C) to make sure the material is well dissolved, resulting in an orange colored solution. DTBP was added to the P3HT solution in small drops and shaken in between to prevent local precipitation. It was then left on the stirrer for another 2 h at room temperature before transferred into a nitrogen glove box (O_2 and H_2O levels <0.1 ppm) for spin-coating. Films for absorption measurements, X-ray diffraction, and XPS measurements were spin-cast on fused silica ("Spectrosil") substrates. For atomic force microscopy, films were deposited on Si/SiO_2-wafer substrates. Glass substrates coated with patterned indium tin oxide of 150 nm thickness were used for solar cell devices. Contact deposition was performed in a high vacuum evaporation chamber ($p = 10^{-6}$ mbar), using a shadow mask to obtain three pixels per substrate each with an active area of 14 mm^2. Absorption measurements were done with a photo-spectrometer (Agilent 8453) and a Veeco Dektak3 surface profiling measurement system was used to determine the film thickness and macroscopic surface roughness. AFM images were recorded with a Veeco Dimension in tapping mode, using NSC35/AIBS ultra sharp cantilevers (MikroMasch Europe).

Grazing incidence X-ray diffraction measurements were performed with a Rigaku Ultima IV type III diffractometer (Rigaku, Tokyo, Japan) equipped with cross beam optics (CBO) by using a Kα wavelength emitted by a Cu anode. Careful alignment of source and detector with respect to the sample was reached by using a thin-film attachment with three degrees of freedom. In order to avoid beam defocusing, the measurements were carried out in parallel beam mode. Divergence of the primary beam was reduced by a 5° Soller slit, while divergence of the diffracted beam was reduced by a 0.5° horizontal Soller slit. The incident angle was kept at 0.5° to avoid any significant scattering from the substrates.

XPS measurements were performed with a ESCALAB IIB spectrometer (VG Scientific Ltd., UK), using the Al Kα line at 1486.6 eV. Pass energy for wide scans was 50 eV and 20 eV for high resolution scans. All the B.E. values are referenced to the aromatic C 1s band at 284.6 eV. Integration of the XPS bands was carried out using the CasaXPS software.

For the characterization of the solar cell devices, the samples were mounted in the glove box to an airtight sample holder and all measurements were performed under medium vacuum conditions. The current–voltage characteristics of the devices were measured using a Keithley source-measure-unit remotely controlled by a computer, and a Sun 3000 Class AAA (Abet Technologies) solar simulator for illumination of the samples. The external quantum efficiency was determined using a setup consisting of a monochromator and a Xenon arc lamp as light source. The wavelength dependent light intensity was monitored by a photodiode to allow the correction of the short-circuit photocurrent after measurement.

For mobility measurements bottom-gate/bottom-contact transistors with the P3HT film as active layer were fabricated. We started from n-doped silicon substrates with a 230 nm SiO_2 layer, patterned with interdigitated ITO (10 nm)/Au (30 nm) source and drain contacts (channel length, $L = 20$ μm and channel width, $Z = 10$ mm, purchased from Fraunhofer Institute IPMS, Dresden, Germany) with an oxygen plasma treatment to increase the Au workfunction. A hexamethyldisilazane (HMDS) layer was spin-coated on the samples, annealed at 100 °C for 1 h and spin-washed with isopropyl alcohol. The transfer characteristics were measured using a Karl Suss PM5 probe station and a HP4145 parameter analyzer, which was connected to low-noise guarded probes for the source- and

drain-contacts and to the probe chuck for the gate connection. For these measurements, the drain-current (I_{DS}) was measured sweeping the gate voltage (V_{GS}) from 20 V to −60 V with a −1 V step and keeping the drain voltage (V_{DS}) constant at −80 V. The HMDS/active-layer deposition and electrical characterization of the TFTs was carried out inside a N_2 glove box.

3. Results and discussion

3.1. Surface morphology

Solutions of 10 mg ml^{-1} P3HT in chlorobenzene were prepared, and a varying amount of DTBP added, up to a DTBP concentration of $c_{DTBP} = 20$ vol%. Films spin-cast from these solutions at 2000 rpm resulted in different thickness, ranging from approximately 25 nm to 60 nm. Fig. 1(a)–(e) show the macroscopic surface profiles of these films, scanned over a distance of 2 mm, and the calculated root mean square roughness R_q. While the profiles for $c_{DTBP} = 0$ vol% and $c_{DTBP} = 3$ vol% are virtually identical, the roughness starts to increase from a concentration of $c_{DTBP} = 9$ vol%. At $c_{DTBP} = 20$ vol%, R_q reaches a value of 8.1 nm with peak heights exceeding 20 nm. A film with such large variation in height is difficult to employ in stacked electronic devices, since it increases the risk to create direct pathways between the electrodes and is difficult to be evened out by following layers. Since this work is motivated by potential applications in solar cells, a further increased film roughness would hardly be acceptable for such applications. Therefore, 20 vol% marks the highest concentration of DTBP used in this work.

More information about the microscopic morphology of the films is obtained with the help of AFM. Fig. 2(a) shows an AFM image of a film spin-cast from a 10 mg ml^{-1} solution of P3HT in chlorobenzene and 14 vol% of DTBP. It shows that the film consists of a network of interwoven fibers, with calculated surface roughness of $R_q = 2.04$ nm (compared to 1.04 nm for a pristine P3HT film prepared under the same conditions, image in ESI†). The single fibers appear to be several micrometers long, but the thickness is not well defined. Besides some "needle-like" features, the main part of the surface appears rather grainy, most probably as a result of non-aggregated polymer chains, which shroud the fibers and hide their actual dimensions. To disentangle the fibers and measure them independently, the solution of preformed fibers was then diluted further to a concentration of 0.005 mg ml^{-1} in chlorobenzene and spin-cast on a silicon dioxide (SiO_2) substrate. In this way it is possible to separate the components of the fiber solution, although it is likely that the formed aggregates get partially redissolved in chlorobenzene. Nevertheless, according to the evolution of UV-vis absorption spectra of the diluted solution monitored over up to 30 min after solution preparation, we found the solution to be essentially stable with just small changes in the high wavelength end of the spectra (see ESI†). We therefore assume that smaller aggregates actually get redissolved, while larger fibers remain mostly unchanged. The AFM image in Fig. 2(b) shows particles of different size, from small dots (~50 nm), to fibers of a length exceeding 2 μm. The measured width and height are similar for all components, being ~40 nm and ~5 nm, respectively, but we have not deconvoluted the images to account for the size and shape of the AFM tip, so the real width is expected to be somewhat smaller. Therefore, the values obtained in the present study are in good agreement with the findings of other groups that used AFM. In addition, using transmission electron microscopy, other groups reported a typical width of around 15–20 nm for P3HT fibers.[21,33]

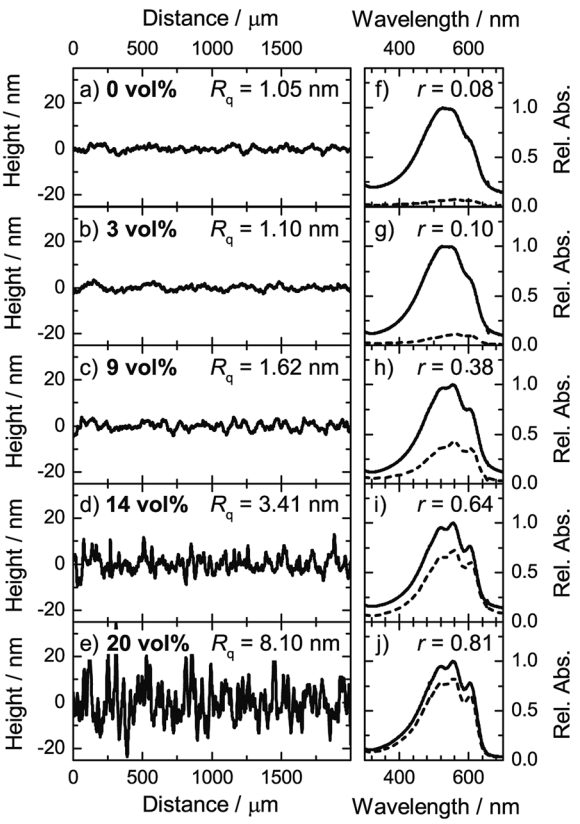

Fig. 1 Macroscopic surface profiles of P3HT films spin-cast from solutions with different DTBP concentration (a)–(e) and associated absorption spectra (f)–(j) of these films before (straight line) and after (dashed line) spin-rinsing with chlorobenzene. R_q is the calculated root mean square roughness of the surface. The film retention factor r is the ratio of the integrated area under the as-cast film and the spin-rinsed film.

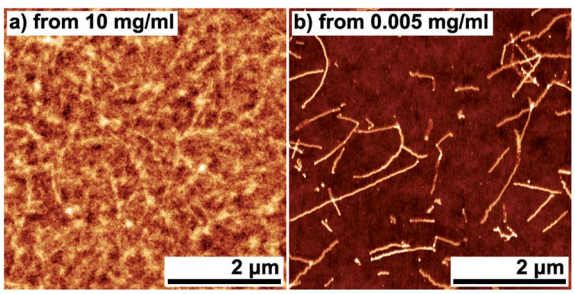

Fig. 2 (a) AFM images of a film spin-cast on a fused silica substrate from a solution of 10 mg ml^{-1} P3HT in chlorobenzene with a 14 vol% content of DTBP. The height-scale is 17 nm. (b) AFM image of P3HT nanofibers on a SiO_2 substrate, spin-cast after further diluting the solution used in (a) to 5×10^{-3} mg ml^{-1} P3HT in chlorobenzene. The height-scale is 6 nm.

3.2. Crystallinity and film retention

Fig. 1(f)–(j) show the UV-vis absorption spectra of the as-cast films (solid lines). Since they were all spin-cast at 2000 rpm, but the viscosity of the solutions increases with increasing DTBP concentration, the film thickness varies, ranging from ~25 nm to ~60 nm, resulting in different values for the absorbance. To enable an easier comparison between the relevant spectral features we have therefore normalized the spectra to the absorption maximum. We also present in Fig. 1 the absorption spectra after the films were "spin-rinsed" with chlorobenzene (dashed lines). "Spin-rinsing" is useful to assess the degree of insolubility of the layer: a drop of chlorobenzene, wetting the whole surface of the substrate, was deposited on the film and after waiting for 1 min spin-rinsed at 2000 rpm. The effect of this procedure is expected to be similar to the deposition of a subsequent layer and therefore a good test for the suitability of the films for bilayer devices. The absorption spectra were divided by the same normalization factor used for the as-cast spectra, allowing a comparison of the spectral shape and intensity.

Comparison of the spectra in Fig. 1(f)–(j) shows that the shape of the absorption of the as-cast films changes considerably with varying peroxide concentration. The spectrum for $c_{DTBP} = 3$ vol% shows one broad absorption peak centered at around 530 nm with a shoulder at 605 nm. For $c_{DTBP} \geq 9$ vol%, the spectrum shows a more pronounced vibrational structure, with transition peaks clearly visible at 520 nm, 555 nm, and 605 nm. The absorption peaks at highest wavelength correspond to the 0–0 and 0–1 transition, and are known to result from weakly coupled H-aggregates.[34,35] The relative intensity of the 0–0 transition peak to the 0–1 transition peak, A_{0-0}/A_{0-1}, is related to the free exciton bandwidth W and can be used as a measure of the degree of crystallinity.[36] Assuming a Huang–Rhys factor of 1,[35] and a negligible change in refractive index for the two transitions,[36] W can be estimated using the equation

$$\frac{A_{0-0}}{A_{0-1}} \approx \left(\frac{1 - 0.24W/E_p}{1 + 0.073W/E_p}\right)^2, \quad (1)$$

where E_p is the energy of the vibrational mode resulting from the symmetric C–C stretch.[36,37] For spin-cast films of P3HT, values typically range from 120 meV to 20 meV, depending on the boiling point of the solvent, film drying conditions, and molecular weight.[38,39] Using A_{0-0}/A_{0-1} from Fig. 1(f)–(j) and $E_p = 180$ meV, we calculated W for the several peroxide concentrations. The values are summarized in Table 1. It shows that both for the case of $c_{DTBP} = 0$ vol% and 3 vol%, A_{0-0}/A_{0-1} is 0.68. For $c_{DTBP} = 9$ vol% and 14 vol%, A_{0-0}/A_{0-1} increases to 0.75 and 0.77, respectively. Interestingly, for an even higher concentration the absorption peak ratio does not increase any further, but stays at 0.77. This value is still relatively small when compared to values reported for highly crystalline films of P3HT and suggests that there is still a significant fraction of the material in a non-aggregated, amorphous phase. This is also supported by the fact that after spin-rinsing, A_{0-0}/A_{0-1} reaches a value of 0.83 for $c_{DTBP} = 9$ vol% and 14 vol% case. This observation clearly demonstrates that it is mainly the amorphous fraction of the film that is washed away, hence the average crystallinity, as represented by A_{0-0}/A_{0-1}, increases.

Table 1 Absorption peak ratio obtained from Fig. 1(f)–(j) and calculated exciton bandwidth W, before and after spin-rinsing the film with chlorobenzene, and the retention factor r, calculated from the absorption spectra as described in the text.

	Before spin-rinsing		After spin-rinsing		
c_{DTBP}/vol%	A_{0-0}/A_{0-1}	W/meV	A_{0-0}/A_{0-1}	W/meV	Retention factor r
0	0.68	99	—	—	0.08
3	0.68	99	—	—	0.10
9	0.75	75	0.84	46	0.38
14	0.77	68	0.83	49	0.64
20	0.77	68	0.79	62	0.81

A retention factor r can be defined as the ratio of the areas under the absorption curve of the as-cast film and spin-rinsed film by integrating from 310 nm to 750 nm. The calculated values for the different films can be found with the absorption spectra in Fig. 1(f)–(g) and are listed in Table 1. We find that the film retention shows a clear dependence on the peroxide concentration, similar to the absorption peak ratio. While in the case of $c_{DTBP} = 3$ vol% just 10% of the material remains on the substrate after spin-rinsing, this value increases to 38%, 64%, and 81% for a c_{DTBP} of 9 vol%, 14 vol%, and 20 vol%, respectively. The fact that the spectrum of the spin-rinsed film of the $c_{DTBP} = 9$ vol% sample shows a higher A_{0-0}/A_{0-1} ratio than the as-cast sample gives evidence that the remaining, insolubilized material consists of a larger fraction of aggregated polymer, and primarily the non-aggregated, amorphous fraction of the film is washed away by the spin-rinsing process. As mentioned above, this results in a high A_{0-0}/A_{0-1} of 0.83 in this case, while this ratio decreases for higher DTBP concentrations.

The fact that the film retention shows the same trend as the surface roughness, *i.e.* an increase with DTBP concentration, suggests that the larger aggregates are primarily responsible for the film becoming insoluble.

As well as from the altered optical absorption, the increased crystallinity caused by the DTBP addition is also evident from X-ray diffraction patterns. Fig. 3 shows the grazing incidence X-ray diffraction (GIXD) spectra of films of pristine P3HT as-cast and after annealing for 10 min at 150 °C, and of P3HT nanofibers formed in a solution with 14 vol% DTBP. All three samples feature a clear diffraction peak at an angle $2\theta = 5.59°$ which can be assigned to the (100) reflection. The intensity of this reflection is highest for the P3HT + DTBP sample and additionally shows the (200) and (300) reflections, which are both absent for the untreated and annealed P3HT samples. Both facts prove the significantly higher degree of crystallinity of the nanofibers compared to the films without DTBP. Using Bragg's law, the distance between the (100) planes can be calculated to be 15.79 Å. It is known that P3HT preferably arranges in an "edge-on" structure, with the polymer chain axis parallel to the substrate surface.[39] The flattened polymer chains form closely packed stacks by interaction of their π-systems along an axis parallel to the substrate surface, forming the fiber axis. A distance of 15.79 Å corresponds to the out-of-plane

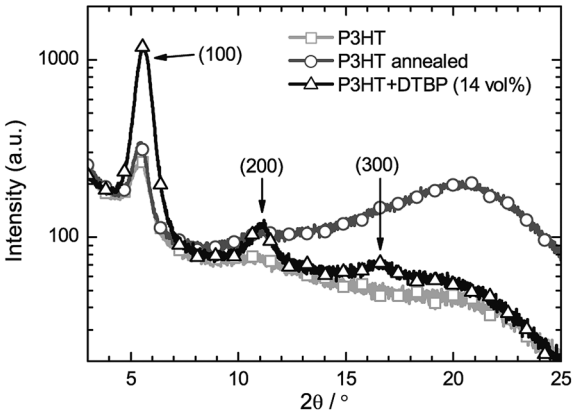

Fig. 3 Grazing incidence X-ray diffraction patterns of films (thickness ~ 50 nm) of pristine P3HT, after annealing at 150 °C for 10 min, and spin-cast from a P3HT + DTBP solution.

lamella stacking distance of P3HT in a Form I configuration, where the hexyl side chains are not interdigitating.[39,40] The π-stacking distance of the polymer chains cannot be probed with the employed setup, but is known to be 3.8 Å for Form I P3HT.[16,39] In contrast to the highly oriented fiber-films, annealing of the P3HT film does not lead to a significant increase of the (100) reflection, but results in a broad halo around $2\theta = 20°$, suggesting the formation of smaller and randomly oriented crystallites.

3.3. Nature of the insolubilization process upon addition of DTBP

The data presented so far all suggest that the process behind the formation of insoluble layers is a self-assembly driven by the limited solubility of P3HT in DTBP. Similar results were reported using other techniques such as slow cooling of P3HT in a marginal solvent or the use of different additives.[15–21] In general, non-polar solvents such as chlorobenzene are well suited for P3HT, which is a non-polar molecule. DTBP in contrast shows a distinct polarity due to the strong electronegativity of the two central oxygen atoms. These two oxygen atoms are relatively weakly bound and responsible for the homolysis of the peroxide, *i.e.* the dissociation of the molecule into two radicals. Because of this process peroxides are commonly used as oxidizing agents. In ref. 30, Gearba and collaborators explain that the peroxide, if added to a solution of P3HT, acts as a radical initiator at elevated temperatures above 100 °C. By attacking mainly the alkyl side chains of P3HT, it can remove hydrogen atoms, leading to bonds between side chains of different polymer strands, while the conjugated system of the polymer backbone remains unaffected. This process would form an interconnected network of polymer chains, resulting in insoluble films. In our case, we see an increase in film retention even without an annealing step. While this is not conclusive evidence for lack of the peroxide homolysis and subsequent cross-linking of the P3HT, we argue that such a process would be extremely unlikely to happen at room temperature, because DTBP is one of the most stable peroxides, consistently with the reported need of a temperature above 100 °C to activate the homolysis. To provide further and corroborating evidence about the effect of DTBP radicals on P3HT, we also kept P3HT films at a temperature of 170 °C in a vapor of DTBP for a varying amount of time (see ESI†). In this case we found that the absorption spectrum loses vibronic structure and shows a blue-shift of the maximum with increasing exposure time, already after a few minutes, consistently with the expected reduction of conjugation length of the system, which should ensue from oxidation of the sulfur in the thiophene rings. Remarkably, however, if the peroxide is added to the solution and kept at room temperature, no sign of oxidation is visible from the UV-vis absorption spectra.

Significantly, also XPS measurements did not provide any indication for the incorporation of additional oxygen in the films upon addition of DTBP to the P3HT solution. In particular, Fig. 4(a) shows how the XPS spectrum of a pure P3HT film compares to a sample where DTBP was added to the solution. Both spectra are virtually identical, clearly showing signals that stem from the 2s and 2p electrons of the sulfur atoms and the carbon 1s signal. In both cases, no signal is detectable at an energy of 530 eV, where the oxygen 1s peak is expected. Furthermore, no sign of oxidation-related groups has been found both in the high resolution spectra of C 1s and S 2p regions for both the analyzed films (Fig. 4(b) and (c)).

Differences of our data with respect to previous literature can be traced back to the different processing temperatures and concentrations, and different material used. Results by Gearba

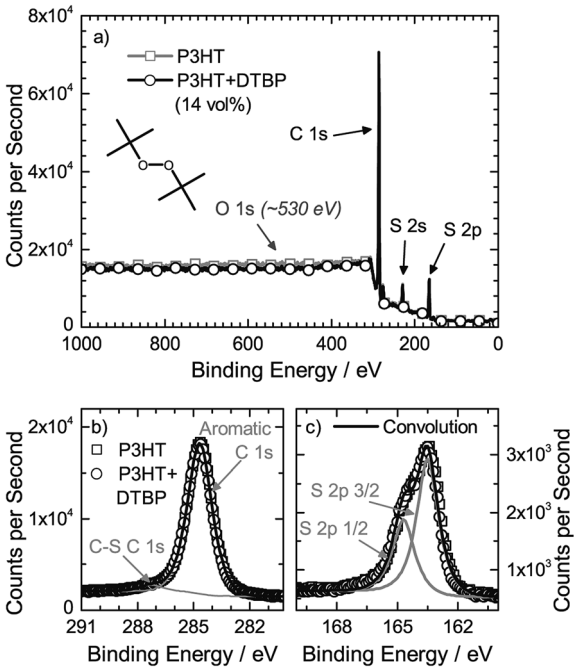

Fig. 4 Wide scan XPS spectra of films spin-cast from solutions with and without DTBP. The arrows mark the signals that are known to stem from carbon and sulfur atoms. The gray arrow and label mark the position where the oxygen 1s signal is expected. Both spectra are virtually identical and show no indication of oxygen. As inset, the chemical structure of DTBP is shown. High resolution scans of the C 1s and S 2p peaks are shown in (b) and (c), respectively. The gray lines show the individual components of the peaks. The overall convolution is shown as black line.

et al. were obtained from a solution with a peroxide concentration >70 radicals per monomer,[30] equivalent to ~40 vol% DTBP for a 10 mg ml^{-1} P3HT solution. That is significantly higher than the one in our work ($c_{DTBP} \leq 20$ vol%), and annealing above 100 °C was performed, rather than processing at room temperature. Such different conditions lead to observation of a blue-shift of the absorption rather than to a growth of a low-energy absorption shoulder, as in our case. However, we are able to observe a blue-shift of the spectrum when annealing our films at 170 °C and in DTBP vapor, which we interpret as an indication of oxidation. In addition, a lower concentration was needed in our case to achieve insolubilization of the layers. This is most likely connected to the different material used, mainly defined by the difference in molecular weight and regioregularity of the P3HT.

In summary, while none of the single pieces of evidence mentioned above provides conclusive evidence sufficient to say that no oxidation is induced by the DTBP, we consider that, taken together, these provide a convincing case to show that DTBP-induced oxidation effects, if any, play a minor role in the formation of P3HT insoluble fibers by this route which is instead driven by the so-called "poor solvent effect". Device data, which we provide below, are entirely consistent with this scenario.

3.4. Thin-film transistors

The influence of DTBP on the charge transport properties was investigated using field-effect transistor measurements. Fig. 5(a) shows the transfer characteristics of the devices, measured in saturation regime ($V_{DS} = -80$ V). It can be seen that the drain–source current I_{DS} for the devices with a high DTBP concentration ($c_{DTBP} \geq 9$ vol%) is larger than for the pure P3HT and $c_{DTBP} = 3$ vol% case. Also, all devices show a high on–off ratio of at least 10^5, although we observe that the off-current (current at 20 V) is increased for the 14 vol% and 20 vol% case.

In saturation regime, I_{DS} is given by

$$I_{DS} = \frac{Z}{2L}\mu C_{Ox}(V_{GS} - V_T)^2, \quad (2)$$

where Z and L are the channel width and length, respectively, μ the field-effect mobility, C_{Ox} the capacitance of the gate dielectric per unit area, V_{GS} the gate voltage, and V_T the threshold voltage.[41] The first derivative of eqn (2) describes a linear dependence of I_{DS} on V_{GS}, with the prefactor defining the slope of the curve. The first derivative of the experimental data can therefore be used to check the validity of eqn (2), as well as to determine the field-effect mobility μ. The data in Fig. 5(b) shows a good linearity for all measured devices.

The second derivative of eqn (2) is the product of the constant ratio of the geometry parameters (Z/L) and the mobility μ. Using the second derivative of the experimental data therefore allows us to calculate the field-dependent mobility, shown in Fig. 5(c). Following the curves from positive to negative V_{GS}, it can be seen that for a high DTBP concentration of 14 vol% and 20 vol% the mobility increases sharply at around +18 V and leads into a flat plateau, ranging from 0 V to −60 V. For pristine P3HT and a low DTBP concentration of 3 vol%, the onset occurs at around +10 V, and the following plateau is tilted. The 9 vol% case shows a somehow intermediate behavior, with an onset at ~10 V and a mainly flat plateau.

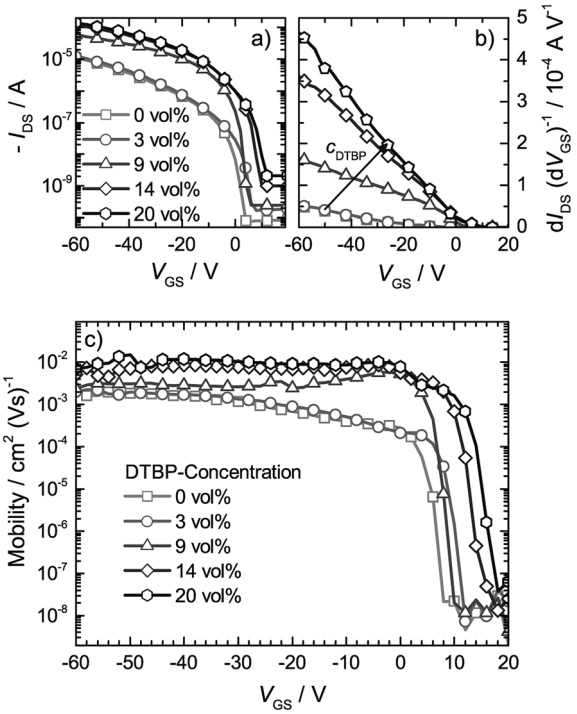

Fig. 5 (a) Transfer characteristics of field-effect transistors fabricated from P3HT solutions with different concentration of DTBP. (b) First derivative of the transfer characteristics shown in (a). (c) Gate-voltage dependence of the mobility for different DTBP concentrations, calculated from the second derivative of the transfer characteristics as shown in (a).

A mobility which is independent of the gate voltage has been correlated to high structural order, as seen when comparing films spun from solvents with different boiling points.[12] An increasing mobility with increasing gate voltage indicates a wide distribution of localized states below the mobility edge of trap states, which get filled with increasing carrier concentration. Clark *et al.* could show that a higher crystallinity results in a narrower trap distribution, hence the weaker dependence on the gate voltage.[38]

It is also very interesting to explore any correlation between mobility and structural parameters, as inferred from spectroscopy. To this end, in Fig. 6(a) we plot the individual values for μ, calculated from a linear fit of the data shown in Fig. 5(b), together with the absorption peak ratio A_{0-0}/A_{0-1} taken from Fig. 1(f)–(j). The values for $c_{DTBP} = 0$ vol% and $c_{DTBP} = 3$ vol% are almost identical, 1.7×10^{-3} cm^2 (V s)$^{-1}$ and 1.8×10^{-3} cm^2 (V s)$^{-1}$, respectively. For higher DTBP concentration, μ starts to increase and reaches a value of 9.9×10^{-3} cm^2 (V s)$^{-1}$ for $c_{DTBP} = 20$ vol%, a more than five-fold increase compared to the case of pure P3HT.

This increase in mobility can be attributed to the altered film morphology associated with the fiber formation discussed in the previous paragraphs. It is known that a high amount of polymer chains in an edge-on orientation can lead to high field-effect mobility.[5] As shown by XRD images above, the

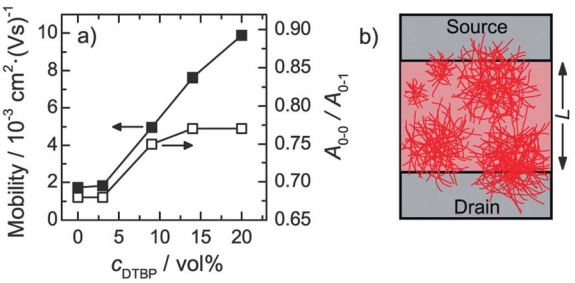

Fig. 6 (a) Mobility in dependence of DTBP concentration, obtained from a linear fit of the curves in Fig. 5(b), and absorption peak ratio A_{0-0}/A_{0-1}, obtained from the curves of the as-cast films (solid lines) in Fig. 1(f)–(j). (b) Schematic of the transistor channel, illustrating how bundles of nanofibers contribute to the charge transport.

polymer chains are highly ordered in π–π stacks along the fiber axis, which, when laid out flat on the surface, puts these polymer chains in an edge-on orientation. The correlation between crystalline quality and mobility can be seen when looking at the trend of the absorption peak ratio A_{0-0}/A_{0-1} in Fig. 6(a). Interestingly, we note that A_{0-0}/A_{0-1} increases significantly from 0 vol % up to 9 vol%, but that a further increase of the DTBP concentration changes this value only marginally, thus suggesting that the fraction of crystalline phase cannot be increased for concentrations greater than 9 vol%. It is intriguing, however, that the mobility keeps increasing beyond the 9 vol% concentration of DTBP, demonstrating that the mobility is a more sensitive probe of the molecular texture than the optical properties are. In particular, we interpret these data as an indication that in addition to the increase in mobility due to the increased average crystallinity also the formation of larger aggregates in the form of fiber networks, plays a significant role. Considering a maximum fiber length of about 2 μm, as shown in the AFM images above, and a channel length of 20 μm, it is clear that the charge transport cannot occur along just a single fiber, but will have to pass fiber junctions. These junctions can be of different type, either overlaps, contacts, or bifurcations, and it has been shown that the measured mobility obtained by field-effect transistor measurements is determined by a complex interplay between the size of the individual networks and the amount and type of junctions.[33,42] The maximum size of the networks in our case can be estimated from the surface topography measurements discussed in Paragraph 2.1. We found that the bundles can be as large as ~25 μm, *i.e.* a similar size as the length L of the transistor channel. Therefore, the interconnectivity of the fibers in form of fiber networks plays an important role for the performance of the thin-film transistor, which is illustrated in a cartoon in Fig. 6(b). Considering the increasing surface roughness with increasing c_{DTBP} and the saturation behavior of the crystallinity, we conclude that the increase in mobility at concentrations $c_{DTBP} > 9$ vol% is most likely to be due to the formation of larger fiber networks, which is beneficial for the charge transport over relatively large distances of several micrometers, consistent with an extensive study of charge transport in P3HT fiber networks by Newbloom and coworkers.[33]

3.5. Solar cells

The possibility to fabricate insoluble films of P3HT allows the subsequent deposition of a second layer, spin-cast from any solvent that is suitable for the material. This is particularly interesting for the use in solar cells using the most common electron acceptor PCBM, since for this material organic solvents such as chlorobenzene or dichlorobenzene, which are good solvents for P3HT as well, are best suited.[43] Although attempts to fabricate P3HT/PCBM bilayer cells from orthogonal solvents led to efficiencies of up to 3.5%,[44] the solubility of PCBM in solvents such as dichloromethane is still poor, which limits the concentration and hence the thickness which can be achieved by spin-casting. In our case, we were able to implement a device architecture where the active layer is formed of a film of P3HT nanofibers and a subsequently deposited layer of PCBM spin-cast from chlorobenzene, as illustrated in Fig. 7(a). The nanofiber solution was prepared using a DTBP concentration of 14 vol%, since this provides a relatively high degree of insolubility while the roughness of the film is still low enough to avoid short circuits (compare Fig. 1(d) and (i)). The P3HT layer was spin-rinsed after deposition to verify the insolubilization and to remove the amorphous fraction at the surface, resulting in a thickness of about 50 nm. The subsequent PCBM layer, spin-cast from a 2 wt% solution in chlorobenzene, has a thickness of about 25 nm. Fig. 7(b) shows the UV-vis absorption spectrum of the bilayer compared to a spectrum of a film of a P3HT:PCBM (1 : 0.8) blend. The increased absorption in the 500–640 nm region due to the crystallinity of the P3HT is preserved after the PCBM deposition, and also after annealing of the bilayer, the absorption spectrum does not change significantly. This suggests that even in the presence of an expected diffusion of PCBM into the P3HT layer, in accordance with previous findings the intermixing mainly takes place in the amorphous P3HT domains, and leaves the crystalline domains unchanged.[8] We would like to point out that although the absorption spectra were measured on films where P3HT and PCBM were deposited directly on a fused silica substrate, we expect the films deposited on PEDOT:PSS to show a similar behavior. Since the fibers

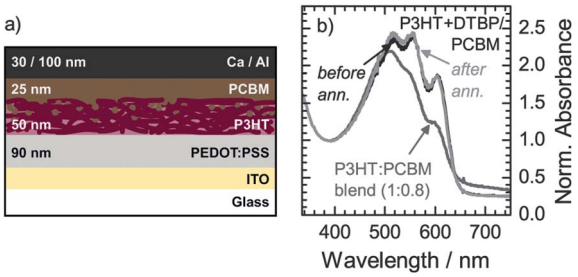

Fig. 7 (a) Schematic of a bilayer solar cell as investigated in this study, comprising a ~50 nm thick film of P3HT nanofibers as absorber layer, and a ~25 nm thick layer of PCBM as electron-accepting layer. The materials are deposited subsequently from the same solvent (chlorobenzene). (b) Normalized absorption spectra of a P3HT/PCBM bilayer on fused silica similar to the one used as active layer in the device shown in (a), before and after annealing at 150 °C. The spectra are compared to a film of a P3HT:PCBM blend (ratio 1 : 0.8). The spectra are normalized to the local minimum at ~395 nm.

are preformed in solution, the substrate will have just a minor influence on the overall crystallinity of the film. The intermixing effects of P3HT and PCBM take place at the interface between the materials, away from the PEDOT:PSS interface, so that the influence of the substrate on this process as well will be negligible. The intermixing of P3HT and PCBM plays an important role in the performance of the device, since it increases the donor–acceptor interface area and can help to form an interpenetrating network beneficial for charge extraction.

Fig. 8(a) shows the current density–voltage (*J–V*) characteristics of three devices with a structure as shown in Fig. 7(a), measured in dark conditions and under a 1000 W m^{-2} AM1.5 illumination. The samples were thermally treated in different ways, either annealed at 150 °C after deposition of the calcium/aluminum cathode (post-annealed), annealed after spin-casting the PCBM layer and before depositing the top contact (pre-annealed), or without any annealing step. In dark conditions, the pre-annealed and the post-annealed device show similar characteristics. Compared to the non-annealed device, it can be seen how annealing at 150 °C changes the slope of the *J–V* curve significantly. The current density in forward bias is significantly increased for both annealed devices, which can be attributed to an improved conduction path for charge extraction, and in particular for electrons owing to rearrangement of PCBM molecules near the interface to the P3HT phase and to the top-contact, as previously suggested.[45,46] The redistribution of PCBM molecules upon annealing also results in a smoothened surface which allows a better contact to the anode and therefore a decreased contact resistance. The smoothening is expected to be more efficient for the pre-annealed device, resulting in a slightly increased current under dark conditions compared to the post-annealed one, although other effects such as specific interactions with the metal electrodes could also play a role.

The improved electron transport also results in an increased fill factor for the post-annealed device compared to the non-annealed device from 40% to 44%, and an increased power conversion efficiency η from 1.3% to 1.6%. However, the short-circuit current (J_{SC}) increases just slightly from 6.2 mA cm^{-2} to 6.8 mA cm^{-2}, indicating that the charge-carrier generation rate is virtually unchanged. In the pre-annealed case, the performance is significantly improved, resulting in a fill factor of 52%, a J_{SC} of 8.4 mA cm^{-2}, and $\eta = 2.3\%$. We consider that the higher J_{SC} indicates a higher charge generation, caused by an increased P3HT/PCBM interface area, since a significant variation due to a difference in the charge extraction paths should also result in more prominent differences in the dark *J–V* characteristics than observed. This scenario is consistent with diffusion of PCBM into the P3HT phase, as also reported by Chen *et al.* by using neutron scattering techniques.[8] Interestingly, the diffusion behavior is strongly influenced by the presence of the top contact, which presumably hinders the movement of the PCBM molecules upon annealing. It is also likely that intermixing already takes places during the deposition of PCBM due to swelling of P3HT in chlorobenzene and a partial removal of amorphous fraction.[46]

Further insight about the morphology can be extracted from the external quantum efficiency (EQE) of the devices, combined with previous literature establishing relevant correlations. Shown in Fig. 8(b) are the spectra for the three different devices discussed above (non-annealed, pre-annealed, post-annealed) in comparison to a typical EQE spectrum of a cell using a P3HT:PCBM (1 : 0.8) blend as active layer. The spectral shapes of the "bilayer" devices are almost identical, while they strongly differ from the blend device. The bilayer spectra feature a plateau between ~400 nm and ~600 nm, while the spectrum of the blend device has a pronounced maximum at ~470 nm. This behavior is caused by a "filter effect" due to the relatively large thickness of the P3HT layer. Incoming light near the absorption maximum of P3HT gets absorbed more strongly before it can reach the P3HT/PCBM interface than light at around the low and high wavelength end of the absorption spectrum.[47] In a blend layer, where the exciton-splitting donor–acceptor interface is distributed through the whole depth of the layer, this filter effect does not show up. It is therefore possible to take the shape of the EQE spectrum as an indicator for how much the morphology matches a "real" bilayer structure, *i.e.* how sharp the interface between donor and acceptor is.[48] Fig. 8(b) shows that there is virtually no difference in the shape of the pre-annealed and the post-annealed device. This indicates that the interdiffusion of the PCBM and P3HT layer happens near the interface, and the PCBM molecules cannot penetrate deeply into the P3HT layer, preserving the multilayer-structure to a large extent. This is in agreement with earlier findings that suggest that the diffusion of the PCBM molecules primarily takes place in the amorphous phase of the P3HT layer, resulting in a morphology similar to film cast from a blend solution already after just seconds of annealing at 150 °C.[8] The high crystallinity of the P3HT in our case prevents this strong interdiffusion.

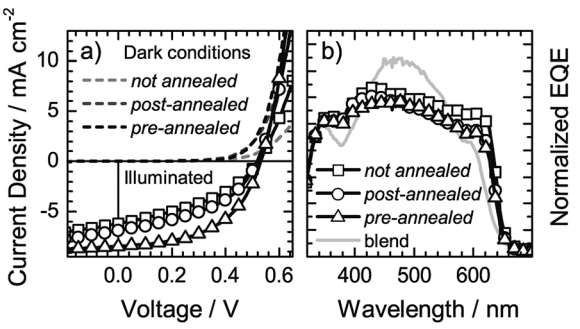

Fig. 8 (a) Current density–voltage characteristics of solar cells with a structure as shown in Fig. 7(a), measured in dark conditions and under illumination by an AM1.5 solar simulator at 1000 W m^{-2}. The devices were either not annealed, or annealed at 150 °C either after cathode deposition (post-annealed), or directly after spin-casting of the PCBM layer, before the cathode was deposited (pre-annealed). (b) External quantum efficiencies (EQE) of the devices shown in (a) and a typical EQE spectrum of a solar cell using a 1 : 0.8 blend of P3HT:PCBM as active layer. The spectra were normalized to allow a better comparison of the shape of the spectra.

4. Conclusions

In summary, we found that the addition of DTBP to a solution of P3HT in chlorobenzene induces a self-assembly process of the

P3HT polymer chains which leads to the formation of semi-crystalline nanofibers of the length of several micrometers. The amount of nanofibers and therefore the average crystallinity can be controlled by adjusting the amount of DTBP added to the solution. We could show increased field-effect mobility, which results from the enhanced crystallinity of the film as well as from the formation of micrometer-sized fiber networks. Formation of such fiber networks also leads to an increase in insolubility, which can be controlled by the DTBP concentration. Insoluble layers of P3HT can be used to fabricate solar cells from successively deposited donor and acceptor layers from the same solvent. After annealing, these devices show a performance comparable to bulk heterojunction solar cells, with a power conversion efficiency of up to 2.3%, while the spectral dependence of the EQE suggests a different morphology due to the limited interdiffusion of P3HT and PCBM caused by the large fraction of aggregated P3HT.

If kept at room temperature, no oxidation effects are apparent from either the UV-vis absorption spectra or XPS spectra in our work, but we do see evidence for oxidation when the films are annealed at 170 °C in DTBP vapor. Most importantly, field-effect transistor measurements powerfully corroborate this interpretation as they show no indication of additional trap states caused by the peroxide.

Acknowledgements

N. S., G. M. L. and F. C. would like to acknowledge funding from the European Union through the Marie Curie initial training network SUPERIOR (PITN-GA-2009-238177) and the NanoSci-E+ project SENSORS. G.M. and G. L. D. acknowledge financial support from the Project PON 2012 "Energetic" (MIUR, Rome).

References

1 L. Dou, J. You, J. Yang, C.-C. Chen, Y. He, S. Murase, T. Moriarty, K. Emery, G. Li and Y. Yang, *Nat. Photonics*, 2012, **6**, 180.
2 Z. He, C. Zhong, X. Huang, W.-Y. Wong, H. Wu, L. Chen, S. Su and Y. Cao, *Adv. Mater.*, 2011, **23**, 4636.
3 Y. Liang, Z. Xu, J. Xia, S.-T. Tsai, Y. Wu, G. Li, C. Ray and L. Yu, *Adv. Mater.*, 2010, **22**, E135.
4 M. Riede, C. Uhrich, J. Widmer, R. Timmreck, D. Wynands, G. Schwartz, W.-M. Gnehr, D. Hildebrandt, A. Weiss, J. Hwang, S. Sundarraj, P. Erk, M. Pfeiffer and K. Leo, *Adv. Funct. Mater.*, 2011, **21**, 3019.
5 H. Sirringhaus, P. J. Brown, R. H. Friend, M. M. Nielsen, K. Bechgaard, B. M. W. Langeveld-Voss, A. J. H. Spiering, R. A. J. Janssen, E. W. Meijer, P. Herwig and D. M. de Leeuw, *Nature*, 1999, **401**, 685.
6 F. Padinger, R. S. Rittberger and N. S. Sariciftci, *Adv. Funct. Mater.*, 2003, **13**, 85.
7 N. D. Treat, M. A. Brady, G. Smith, M. F. Toney, E. J. Kramer, C. J. Hawker and M. L. Chabinyc, *Adv. Energy Mater.*, 2011, **1**, 145.
8 D. Chen, F. Liu, C. Wang, A. Nakahara and T. P. Russell, *Nano Lett.*, 2011, **11**, 2071.
9 D. M. DeLongchamp, B. M. Vogel, Y. Jung, M. C. Gurau, C. A. Richter, O. A. Kirillov, J. Obrzut, D. A. Fischer, S. Sambasivan, L. J. Richter and E. K. Lin, *Chem. Mater.*, 2005, **17**, 5610.
10 A. Zen, J. Pflaum, S. Hirschmann, W. Zhuang, F. Jaiser, U. Asawapirom, J. P. Rabe, U. Scherf and D. Neher, *Adv. Funct. Mater.*, 2004, **14**, 757.
11 J.-M. Verilhac, G. LeBlevennec, D. Djurado, F. Rieutord, M. Chouiki, J.-P. Travers and A. Pron, *Synth. Met.*, 2006, **156**, 815.
12 J. F. Chang, B. Q. Sun, D. W. Breiby, M. M. Nielsen, T. I. Solling, M. Giles, I. McCulloch and H. Sirringhaus, *Chem. Mater.*, 2004, **16**, 4772.
13 H. C. Yang, T. J. Shin, L. Yang, K. Cho, C. Y. Ryu and Z. N. Bao, *Adv. Funct. Mater.*, 2005, **15**, 671.
14 H. H. Yang, S. W. LeFevre, C. Y. Ryu and Z. N. Bao, *Appl. Phys. Lett.*, 2007, **90**, 172116.
15 K. J. Ihn, J. Moulton and P. Smith, *J. Polym. Sci., Part B: Polym. Phys.*, 1993, **31**, 735.
16 J. A. Merlo and C. D. Frisbie, *J. Phys. Chem. B*, 2004, **108**, 19169.
17 S. Berson, R. De Bettignies, S. Bailly and S. Guillerez, *Adv. Funct. Mater.*, 2007, **17**, 1377.
18 N. Kiriy, E. Jahne, H. J. Adler, M. Schneider, A. Kiriy, G. Gorodyska, S. Minko, D. Jehnichen, P. Simon, A. A. Fokin and M. Stamm, *Nano Lett.*, 2003, **3**, 707.
19 Y. D. Park, H. S. Lee, Y. J. Choi, D. Kwak, J. H. Cho, S. Lee and K. Cho, *Adv. Funct. Mater.*, 2009, **19**, 1200.
20 A. J. Moule and K. Meerholz, *Adv. Mater.*, 2008, **20**, 240.
21 L. Li, G. Lu and X. Yang, *J. Mater. Chem.*, 2008, **18**, 1984.
22 B.-G. Kim, M.-S. Kim and J. Kim, *ACS Nano*, 2010, **4**, 2160.
23 A. R. Aiyar, J.-I. Hong, R. Nambiar, D. M. Collard and E. Reichmanis, *Adv. Funct. Mater.*, 2011, **21**, 2652.
24 A. Charas, H. Alves, J. M. G. Martinho, L. Alcacer, O. Fenwick, F. Cacialli and J. Morgado, *Synth. Met.*, 2008, **158**, 643.
25 O. Fenwick, K. Oliver and F. Cacialli, *Appl. Phys. Lett.*, 2012, **100**, 053309.
26 X. C. Li, T. M. Yong, J. Gruner, A. B. Holmes, S. C. Moratti, F. Cacialli and R. H. Friend, *Synth. Met.*, 1997, **84**, 437.
27 R. Q. Png, P. J. Chia, J. C. Tang, B. Liu, S. Sivaramakrishnan, M. Zhou, S. H. Khong, H. S. O. Chan, J. H. Burroughes, L. L. Chua, R. H. Friend and P. K. H. Ho, *Nat. Mater.*, 2010, **9**, 152.
28 G. Winroth, G. Latini, D. Credgington, L. Y. Wong, L. L. Chua, P. K. H. Ho and F. Cacialli, *Appl. Phys. Lett.*, 2008, **92**, 103308.
29 C. Tao, M. Aljada, P. E. Shaw, K. H. Lee, H. Cavaye, M. N. Balfour, R. J. Borthwick, M. James, P. L. Burn, I. R. Gentle and P. Meredith, *Adv. Energy Mater.*, 2013, **3**, 105.
30 I. R. Gearba, C. Y. Nam, R. Pindak and C. T. Black, *Appl. Phys. Lett.*, 2009, **95**, 173307.
31 A. G. Andreopoulos and E. M. Kampouris, *J. Appl. Polym. Sci.*, 1986, **31**, 1061.
32 T. K. Kang and C. S. Ha, *Polym. Test.*, 2000, **19**, 773.
33 G. M. Newbloom, F. S. Kim, S. A. Jenekhe and D. C. Pozzo, *Macromolecules*, 2011, **44**, 3801.
34 X. M. Jiang, R. Osterbacka, O. Korovyanko, C. P. An, B. Horovitz, R. A. J. Janssen and Z. V. Vardeny, *Adv. Funct. Mater.*, 2002, **12**, 587.

35 F. C. Spano, *J. Chem. Phys.*, 2005, **122**, 234701.
36 J. Clark, C. Silva, R. H. Friend and F. C. Spano, *Phys. Rev. Lett.*, 2007, **98**, 206406.
37 F. C. Spano, J. Clark, C. Silva and R. H. Friend, *J. Chem. Phys.*, 2009, **130**, 074904.
38 J. Clark, J.-F. Chang, F. C. Spano, R. H. Friend and C. Silva, *Appl. Phys. Lett.*, 2009, **94**, 163306.
39 M. Brinkmann, *J. Polym. Sci., Part B: Polym. Phys.*, 2011, **49**, 1218.
40 W. D. Oosterbaan, V. Vrindts, S. Berson, S. Guillerez, O. Douheret, B. Ruttens, J. D'Haen, P. Adriaensens, J. Manca, L. Lutsen and D. Vanderzande, *J. Mater. Chem.*, 2009, **19**, 5424.
41 G. Horowitz, *Adv. Mater.*, 1998, **10**, 365.
42 G. M. Newbloom, K. M. Weigandt and D. C. Pozzo, *Macromolecules*, 2012, **45**, 3452.
43 P. A. Troshin, H. Hoppe, J. Renz, M. Egginger, J. Y. Mayorova, A. E. Goryochev, A. S. Peregudov, R. N. Lyubovskaya, G. Gobsch, N. S. Sariciftci and V. F. Razumov, *Adv. Funct. Mater.*, 2009, **19**, 779.
44 A. L. Ayzner, C. J. Tassone, S. H. Tolbert and B. J. Schwartz, *J. Phys. Chem. C*, 2009, **113**, 20050.
45 A. Kumar, G. Li, Z. Hong and Y. Yang, *Nanotechnology*, 2009, **20**, 165202.
46 D. Chen, A. Nakahara, D. Wei, D. Nordlund and T. P. Russell, *Nano Lett.*, 2011, **11**, 561.
47 Assuming a P3HT layer thickness of 40 nm and an absorption coefficient of 0.005 nm^{-1} at 470 nm and 0.001 nm^{-1} at 600 nm, gives a 45% higher intensity of 600 nm photons compared to 470 nm photons after light has travelled through this layer.
48 V. S. Gevaerts, L. J. A. Koster, M. M. Wienk and R. A. J. Janssen, *ACS Appl. Mater. Interfaces*, 2011, **3**, 3252.